Interferometric amplitude apodization of integrated gratings

T. W. Mossberg, C. Greiner, and D. Iazikov

LightSmyth Technologies, Inc., 860 W. Park St. Ste 250, Eugene, OR 97041
twmoss@LightSmyth.com

http://www.LightSmyth.com

Abstract: Modern photolithography with its sub-hundred-nanometer-scale resolution and cm-scale spatial coherence provides for the creation of powerful waveguide diffractive structures useful as integrated spectral filters, multiplexers, spatial signal routers, interconnects, etc. Application of such structures is facilitated by a lithographically friendly means of amplitude apodization, which allows for programming of general spectral and spatial transfer functions. We describe here an approach to implementing flexible binary-etch-compatible diffractive amplitude control based on the decomposition of diffractive structures into subregions each of whose diffractive contours are spatially positioned so as to interferometrically control the net diffractive amplitude and phase of the subregion. The present approach is uniquely powerful because it allows for substantial decoupling of amplitude and phase apodization.

OCIS codes: (050.1950) Diffraction gratings, (230.7380) Waveguides, channeled, (130.2790) Guided waves, (220.4000) Microstructure fabrication, (230.1480) Bragg reflectors

References and links

1. C. Greiner, D. Iazikov, and T. W. Mossberg, "Lithographically-fabricated planar holographic Bragg reflectors," J. Lightwave Technol. **22**, 136-145 (2004).
2. J. L. Rebola and A. V. T. Cartaxo, "Performance optimization of Gaussian apodized fiber Bragg grating filters in WDM systems," J. Lightwave Technol. **8**, 1537-1544 (2002).
3. T. Komukai, K. Tamura, and M. Nakazawa, "An efficient 0.04-nm apodized fiber Bragg grating and its application to narrow-band spectral filtering," IEEE Photonics Technol. Lett. **9**, 934-936 (1997).
4. T. Erdogan, "Fiber grating spectra," J. Lightwave Technol. **15**, 1277-1294 (1997).
5. D. Wiesmann, C. David, R. Germann, D. Erni, and G. L. Bona, "Apodized surface-corrugated gratings with varying duty cycles," IEEE Photonics Technol. Lett. **12**, 639-641 (2000).
6. D. Wiesmann, R. Germann, G. L. Bona, C. David, D. Erni, and H. Jackel, "Add-drop filter based on apodized surface-corrugated gratings," J. Opt. Soc. Am. B **20**, 417-423 (2003).
7. D. Iazikov, C. Greiner, and T. W. Mossberg, "Effective gray scale in lithographically scribed planar holographic Bragg reflectors," Appl. Opt. **43**, 1149-1153 (2004).
8. C. Greiner, T. W. Mossberg, and D. Iazikov, "Bandpass engineering of lithographically-scribed channel-waveguide Bragg gratings," Opt. Lett. **29**, 806-808 (2004).
9. B. Malo, S. Theriault, D. C. Johnson, F. Bilodeau, J. Albert, K. O. Hill, "Apodisation of the spectral response of fibre Bragg gratings using a phase mask with variable diffraction efficiency," Electron. Lett. **31**, 223 – 225 (1995).
10. H. J. Deyerl, N. Plougmann, J. B. Jensen, F. Floreani, H. R. Sørensen, M. Kristensen, "Fabrication of Advanced Bragg Gratings with Complex Apodization Profiles by Use of the Polarization Control Method," Appl. Opt. **43**, 3513-3522 (2004).
11. M. Ibsen, M. K. Durkin, M. J. Cole, R. I. Laming, "Sinc-sampled fiber Bragg gratings for identical multiple wavelength operation," Photonics Technology Lett. **10**, 842 - 844 (1998).

#6642 - $15.00 US Received 22 February 2005; revised 11 March 2005; accepted 17 March 2005

It has recently been demonstrated [1] that deep ultraviolet (DUV) photolithography provides a powerful means of producing distributed diffractive or holographic structures in slab and channel waveguides providing for the fabrication of virtually arbitrary computer-designed patterns pixilated at the resolution of <100 nm with full spatial coherence on the centimeter scale. Such flexible fabrication means allow for the incorporation of powerful volume holographic design concepts into distributed diffractive structures providing for general spatial and spectral signal processing, filtering, and routing in device formats consistent with high volume and low-cost production. In the present work, we explore the application of DUV photolithographic design flexibility to the realization of an amplitude and phase apodization means that is fully compatible with fabrication friendly binary etch methods and at the same time uniquely minimizes the coupling of amplitude and phase effects. The present method, correlated-contour apodization, utilizes the precise placement of contours within diffractive contour subsets to interferometrically control the amplitude and phase of the net field diffracted by the contour subset. We note that other apodization methods have been demonstrated in fiber Bragg gratings [2-4], channel waveguides [5,6] and slab diffractive structures [7]. These previously described methods generally introduce a complex coupling between amplitude and phase apodization.

Correlated-contour amplitude and phase control is applicable to many distributed diffractive structures including channel waveguide Bragg gratings, slab waveguide holographic Bragg reflectors (HBRs), and even free-space reflection and transmission gratings. A lithographically-scribed channel waveguide grating is depicted schematically in Fig. 1 from a top view (1(a)) and side view (1(b)). The diffractive contours (lines) of the grating are patterned with a deep ultraviolet (DUV) stepper in resist, etched into the channel waveguide core, and filled with material of differing refractive index. A top view of a holographic Bragg reflector (HBR) is shown in Fig. 1(c). The HBR is a volume hologram implemented in a slab waveguide. Light typically enters the slab region through a channel waveguide and then expands freely (in the plane) to interact with the curved HBR diffractive contours. The shape of each contour may be computer-tailored to create from the input signal an output signal whose wavefront is optimally matched to the entry mode of the output channel waveguide. Simple geometric curves like circles and ellipses may suffice for coupling between input and output ports in some cases, but custom contours (like aspheric

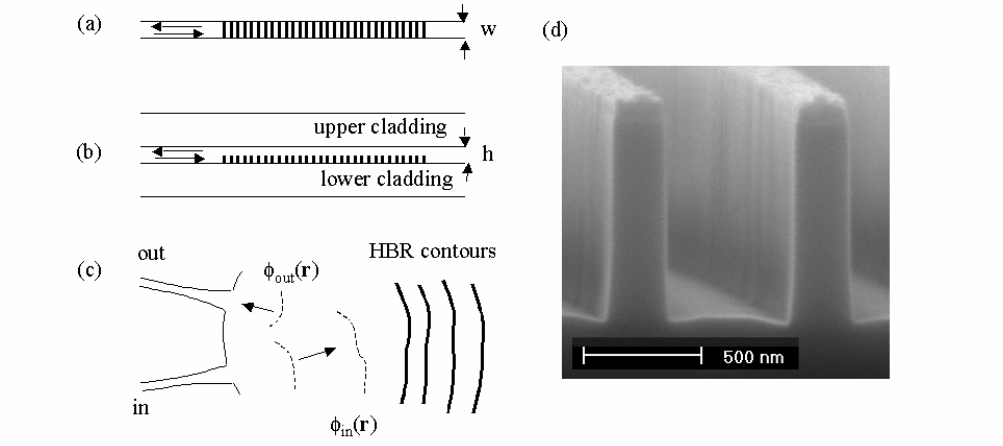

Fig. 1. (a)-(b) Top and side views of channel waveguide grating, respectively. (c) Top-view of slab-waveguide holographic Bragg reflector with channel waveguide access. (d) Photograph of grating contours for channel waveguide grating prior to fill.

#6642 - $15.00 US Received 22 February 2005; revised 11 March 2005; accepted 17 March 2005

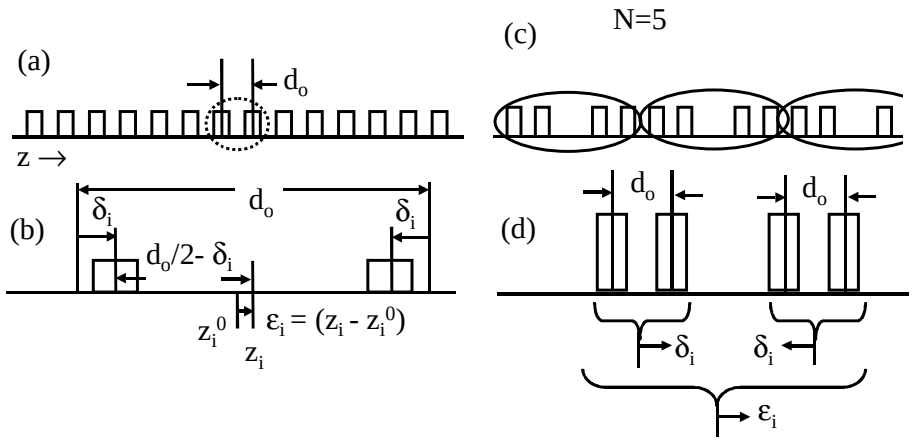

Fig, 2. Basic concept of correlated-contour amplitude and phase control. (a) Uniform grating. (b) Blow-up of two adjacent grating contours with common and differential position shifts. (c) Five-contour subgroups with center contour deletion to provide room for centerwise displacement of outer contours. (d) Common mode and differential displacements of contour set elements (N=5) used to adjust phase and amplitude, respectively.

imaging optics) will provide more efficient signal coupling in general HBR designs. With modern DUV photolithographic fabrication, aspherics are as easy to fabricate as spherics. The various contours of the HBR are spaced so that generated output wavefronts from the ensemble arrive at the output port with designed phase relationships and typically a common wavefront. Correlated-contour apodization comprises spatial repositioning of contours within contour subsets so that the coherent addition of their scattered wavefronts is adjusted to desired values. Overall phase shifts can be implemented through spatial shifts in the center of gravity of the various contour subsets. Figure 1(d) is a scanning-electron microscope picture of diffractive contours like those used in the channel waveguides prior to filling with cladding.

There are many ways a collection of diffractive contours can be positionally dispersed to achieve a desired net reflectivity. We concentrate here on one specific but systematic approach to contour positioning. In Fig. 2(a), we depict a grating structure of constant spacing d_o, which will backscatter light at wavelength $\lambda_o = 2nd_o$, where n is the effective waveguide refractive index. We assume that the overall bandwidth of the grating $\Delta\lambda$ is very small compared to λ_o (i. e. $\Delta\lambda/\lambda_o << 1$). In Fig. 2(b), we show a two-member set of diffractive contours. If the central position of the set is z_i^o (z_i) prior to (after) apodization, and the final separation between lines is $d_i = d_o - 2\delta_i$, with the contours symmetric about z_i (see Fig. 2(b)), the net field backscattered from the line pair will be

$$E_i(\delta_i, \varepsilon_i) = E_o \exp(2ik_o\varepsilon_i)\cos(2k_o\delta_i)\,, \tag{1}$$

where E_o is the net backscattered field magnitude from the set of two correlated lines for resonant light with $\delta_i = 0$, $k_o = 2\pi n/\lambda_o$, $\varepsilon_i = z_i - z_i^o$, and it is assumed that $k_o d_o = m\pi$ (m=1,2,…). The two parameters δ_i and ε_i, provide independent control over the net reflective amplitude and phase, respectively, of the correlated two-line set. The resonant correlated-line-set amplitude reflection coefficient may be written as

#6642 - $15.00 US Received 22 February 2005; revised 11 March 2005; accepted 17 March 2005

$$\rho(\delta_i) = \frac{E_i(\delta_i)}{E_o} = \cos(2k_o\delta_i) \tag{2}$$

The reflected field amplitude, being interferometrically determined, exhibits chromatic variation. But in the limit of $\Delta\lambda/\lambda_o << 1$, the amplitude of the apodized line pair will be essentially constant over the reflection bandwidth of the overall grating. To provide a many-line grating with smooth reflective amplitude variation along its length, all diffractive contours in the grating are grouped into line pairs with δ_i and ε_i variable from pair to pair.

A unique feature of the correlated-contour apodization method is that the surface-etch percentage, averaged over distances $>>\lambda_o$, remains nominally constant allowing the guided waves to experience a constant average material composition. This ideal situation can be complicated by fabrication imperfections, for example involving etch-profile changes with neighbor separation. Such effects are shown here to be small. Owing to the nominally constant material composition, the effective waveguide refractive index n may be expected to remain essentially constant as the diffractive amplitude is changed. In this case, phase modulation is not intrinsically coupled to amplitude apodization. In previously described amplitude apodization methods applicable to etched gratings [2-8], amplitude changes typically introduce changes in average material composition and hence in n. Changes in n, unless compensated in design, have the effect of introducing position-dependent phase shifts concomitant to intended amplitude apodization. Coupling of phase and amplitude apodization can significantly complicate the problem of achieving desired grating response. We note that decoupling of amplitude apodization from index variation has been developed previously for gratings based on photo-written index variations [9-11].

In some cases, the spacing between grating lines, d_o, may be at the level of lithographic resolution, which implies that displacements of contours toward one another cannot be correctly rendered. In this scenario (applicable to our experiments), correlated-contour amplitude apodization can be implemented as shown in Figs. 2(c-d). The contours, in the case shown, are divided into groupings of 5 lines each. The center line of each set is deleted (Fig. 2(c)). Deletion of the center line provides room for the lines on each side to be moved toward the center of the original group, as shown in Fig. 2(d), while leaving a lithographically renderable gap. The center-line deletion approach can be extended to correlated line sets involving an arbitrary (initially) odd number, N, of diffractive contours. As we implement the method, all lines on either side of the center are displaced symmetrically in a manner analogous to that shown in Fig. 2(d). The reflected amplitude and phase of the groupings then still varies as in Eqs. (1-2), where E_o represents the $\delta_i=0$ reflection amplitude of a correlated set regardless of the number of lines involved. Deletion of the center line of each contour grouping may introduce additional grating resonances. With deleted lines, the grating can be viewed as a first-order grating as in Fig. 2(a) combined with an oppositely signed N^{th}-order grating with the latter having resonances spaced about k_o by k_o/N. For small values of N and thus wide spectral spacing the additional resonances can typically be ignored. Alternatively, by varying N throughout the diffractive structure, the additional resonances may be reduced in amplitude as needed.

We have tested correlated-contour diffractive amplitude control in both channel waveguides and HBRs. All guiding structures fabricated are multilayer silica-on-silicon. The HBR structures have a 2-μm thick core with bilateral 15 μm cladding and core-cladding refractive index contrast of 0.8 percent. Diffractive structures are patterned (via DUV photolithography) and etched on the top of the core layer to a depth of about 450 nm and filled with cladding. HBR diffractive contours are circular with input and output waveguides at common conjugate image points. The HBR contours span an area of approximately 2×2 mm and contain about 4000 contours. The channel waveguide structures employed have core dimensions of approximately 2×6 μm and differed from the HBR structures in that the

#6642 - $15.00 US Received 22 February 2005; revised 11 March 2005; accepted 17 March 2005

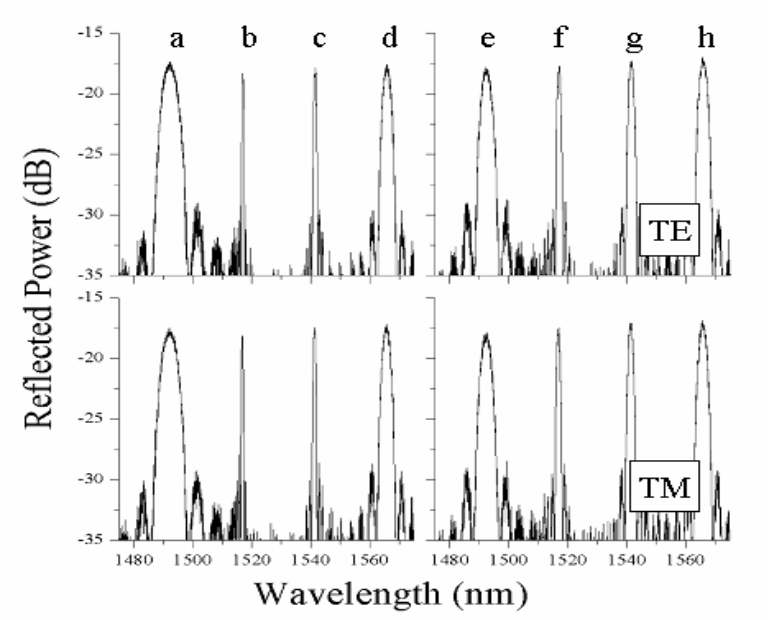

Fig. 3. Reflection spectra of two channel waveguides (left and right) each containing four separate gratings. Top and bottom rows show different input polarizations. Each individual grating is written with identical contour sets adjusted to specific field reflectivity and grating lengths are adjusted to provide nearly uniform net reflectivity (see text).

core was comprised of two sublayers with diffractive contours etched 850 nm deep into the top of the 1-μm –thick lower core layer (2 percent index contrast relative to the cladding) and filled with the upper core layer (0.8 percent contrast relative to the cladding). Channel diffractive contours are straight segments oriented normal to the channel propagation direction and spanning the entire transverse extent of the guide. The channel waveguide core was surrounded by lower index cladding. All diffractive structures were designed to operate in the weak reflection limit (< 10 percent power reflection) to eliminate saturation effects. Operation in the weak reflection limit is for experimental convenience only. Measurement in this limit allows for strict proportionality between the reflectivity of individual correlated-line sets and the easily measured reflectivity of a whole grating comprised of many correlated sets.

To test the variation of reflectivity and refractive index with line displacement (δ_i), eight separate channel waveguide gratings were fabricated. The channel waveguide gratings utilized 5-line (center-line-deleted) correlated-line-set amplitude control (see Fig. 2(d)). Within each grating, δ_i (the line displacement) was held constant. The number of correlated line sets within each grating was varied so that the overall grating reflectivity (number of correlated sets × individual set reflectivity) was held approximately constant providing a convenient nearly constant reflected power level for measurement. The gratings were located sequentially, without spatial overlap, along two channel waveguides with gratings (a-d) in one channel and (e-h) in the other. Gratings within a single channel were displaced in wavelength so that they could be distinguished in the reflective measurement. Wavelength separation was set large to avoid interference. More generally, wavelength separation may be varied continuously in increments down to the transform limit. In Fig. 3, we show the reflection spectra of the gratings. Reflected powers include a 7 dB excess input coupling loss unique to the test setup. The top and bottom of Fig. 3 detail the grating responses to TE and TM input polarizations, respectively. The design physical characteristics of the various

#6642 - $15.00 US Received 22 February 2005; revised 11 March 2005; accepted 17 March 2005

gratings are given in Table 1. Note the variations in grating resonance width resulting from the variation in overall length from grating to grating. This width variation is expected for spatially coherent gratings.

Table 1. Channel Waveguide Grating Properties

Grating	Line Spacing d_0 (μm)	Line Set Number	δ_i/d_0	Relative Amplitude Reflectivity ρ	Expected Grating Reflectivity (Power (dB))	Measured Wavelength (nm)
a	0.511816	47	0	1.00	0	1492.296
b	0.520404	461	0.234	0.10	-0.136577	1517.006
c	0.528991	283	0.2245	0.16	-0.349022	1541.486
d	0.537579	89	0.1665	0.50	-0.459022	1565.915
e	0.511816	66	0.1245	0.71	-0.034176	1492.373
f	0.520404	210	0.2145	0.22	-0.101551	1516.990
g	0.528991	141	0.198	0.32	-0.329000	1541.518
h	0.537579	89	0.1665	0.50	-0.459022	1565.945

The observed reflected powers are converted to fields and are normalized by the number of contour sets in each grating to arrive at a measured correlated-set amplitude reflectivity. Identical gratings appearing in both channel waveguides are used to normalize out reflectivity variations introduced by differences in fiber-to-channel coupling. In Fig. 4, measured amplitude reflectivity is plotted versus Eq. (2) reflectivity. The agreement between designed and measured contour-set amplitude reflectivities is quite good indicating that the fabrication process provides high fidelity and that the underlying theory is sound. Some deviation from Eq. (2) is expected because the lithographic process exhibits some fidelity

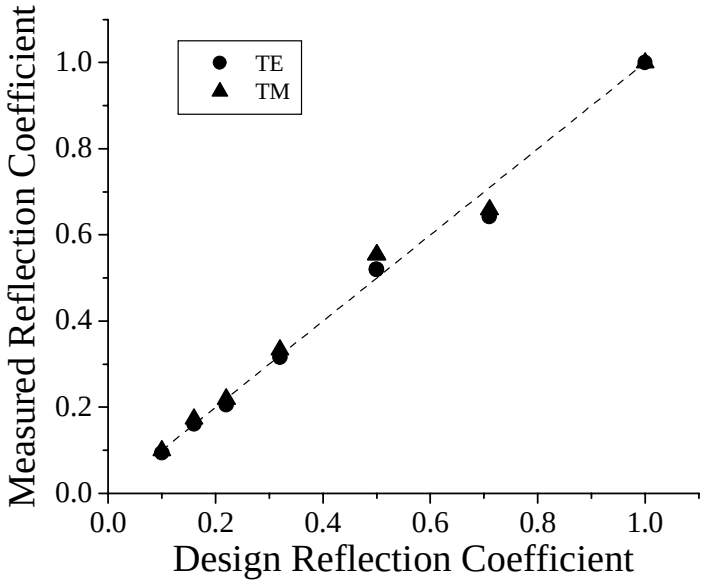

Fig. 4. Plot of measured amplitude reflection coefficient versus design reflection coefficient for the gratings of Table 1.

#6642 - $15.00 US Received 22 February 2005; revised 11 March 2005; accepted 17 March 2005

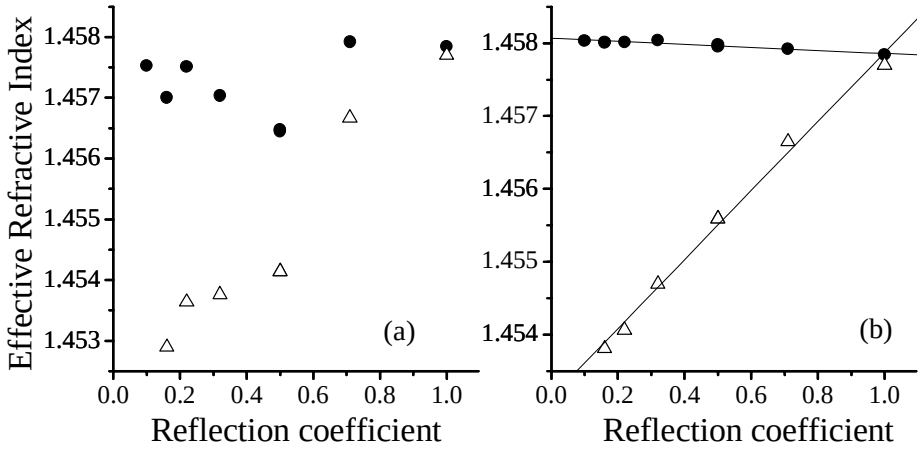

Fig. 5. (a) Measured effective refractive index as a function of amplitude reflection coefficient for correlated-line-set gratings (solid circles) and a reference grating set (open triangles) whose reflectivity is controlled via the partial scribe method of Ref. 8. (b) Effective refractive index of the two grating sets after extracting intrinsic wavelength dependence.

variation as the pattern rendered is varied. As seen from Fig. 4, complications of this kind are relatively small. Ultimately, an empirical replacement for Eq. (2) may be devised that accounts for fabrication subtleties as necessary.

The data of Fig. 4 indicates that correlated-contour apodization is effective in controlling the reflective amplitude of gratings. We now examine how effective refractive index varies with the reflective amplitude. To investigate this issue, we plot index values derived from the eight test gratings as determined by measuring the peak reflected wavelength, λ_o, for each channel waveguide grating, using the parameters of Table I, and applying the relation $n = \lambda_o / 2d_o$. Resulting index values are plotted (solid points) in Fig. 5(a) as a function of design grating reflectivity. Also plotted as the open triangles, are the similarly derived effective indices for a reference set of channel waveguide gratings whose reflection amplitude is varied using the partial-fill grayscale method [8]. In the partial-fill grayscale method, reflective amplitude is varied by adjusting the width of the grating lines across the channel waveguide. As the width of grating lines varies, the amount of fill material added varies. Thus the average material composition seen by signals changes with reflective amplitude and a significant correlation of amplitude and index may be expected. This reference set of gratings spans a range of wavelengths and reflectivities similar to the correlated-line-set gratings.

Geometric and material properties lead to a natural variation of effective waveguide index as a function of signal wavelength. Since the test gratings are displaced in wavelength, the raw index data of Fig. 5(a) should be corrected to remove natural wavelength related changes. We have done this using measured material and estimated geometric index effects and plot the corrected grating indices in Fig. 5(b). It is clear that the coupling between reflective amplitude and effective index is much weaker for gratings apodized using the correlated-contour amplitude control method than for those apodized using the partial-fill method. With correlated-contour amplitude control, absolute index changes on the level of only a few parts in 10^4 are observed when reflective amplitude is varied over an order of magnitude. It should be noted that the design reflectivity of the correlated-contour test gratings does not vary monotonically with wavelength (see Table I). It is for this reason that

#6642 - $15.00 US Received 22 February 2005; revised 11 March 2005; accepted 17 March 2005

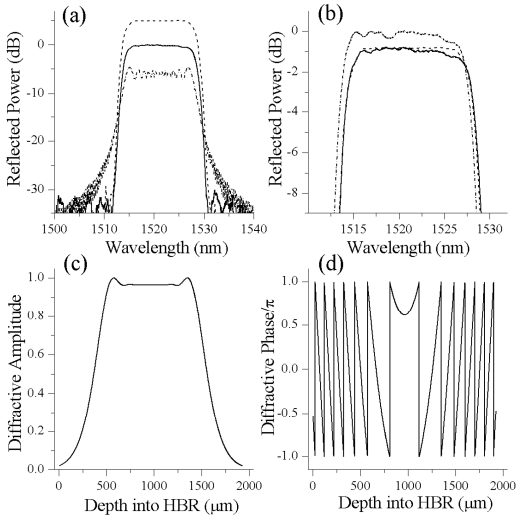

Fig. 6. Reflection spectra of HBRs apodized with 3-line (N=3) correlated-contour amplitude and phase control. In (a), the lower trace depicts the calculated reflective spectrum of a linearly chirped grating with no amplitude apodization, the middle (solid) trace is a measured reflection spectrum of an apodized HBR, the top trace (dashed) is the simulated HBR response, which is displaced upward by 5 dB for clarity. (b) is a blow-up of the measured reflection spectrum of part (a) with traces (TE top) for both polarizations and scalar simulated spectrum (flattest). The amplitude and phase apodization functions employed in the HBR of (a-b) are shown in (c) and (d), respectively.

the wiggles in the index data of Fig. 5(a) are smoothed (as shown in Fig. 5(b)) when one corrects for the natural waveguide chromatic index variation.

In Fig. 6, we show the reflection spectra of HBR filters designed to produce flat-top passbands approximately suitable for course WDM multiplexing. Fig. 6(a) (solid line), depicts the TM reflection spectrum of an HBR apodized with correlated-contour apodization (N=3). The dashed line is the design bandpass function (displaced by 5 dB above the measurement for display). The vertical scale of Fig. 6(a) is expanded in Fig. 6(b) where TE (top), TM (bottom), and design (flattest) bandpass functions are shown. Figure 6(c) (6(d)) shows the radial amplitude (phase) apodization function employed in the HBR. The phase function shown corresponds approximately to a linear period chirp. Measurements of empty channel waveguides indicate that coupling to the rectangular access channels accounted for nearly all of the change in reflected power with polarization observed in Fig. 6(b). Slight ripple in the observed passband may have occurred because of coherent backscattering from edges and other structures within the test die. The oscillating bandpass function (lowest curve) shown in Fig. 6(a) shows the calculated reflection spectrum from a linearly chirped grating of constant amplitude (unapodized). Overall, it is clear that the correlated contour apodization approach allows for powerful passband control.

We have described an approach to introducing position-dependent diffractive amplitude and phase into distributed diffractive structures. The method is enabled by the precise and arbitrary positioning control afforded to designers by DUV photolithography and waveguide deposition techniques. Advanced integrated filtering and signal processing devices of diverse character are enabled by the spectral and spatial programmability the present apodization approach allows. We note that the present apodization method may be applied even in the case of free-space surface gratings.

#6642 - $15.00 US Received 22 February 2005; revised 11 March 2005; accepted 17 March 2005